Solid State Sciences 141 (2023) 107211

Contents lists available at ScienceDirect

Solid State Sciences

journal homepage: www.elsevier.com/locate/ssscie

Study of structural, elastic, mechanical, electronic and magnetic properties of FeX (X=Pt, Pd) austenitic and martensitic phases

Z. Zerrougui [a], K. Bouferrache [b], M.A. Ghebouli [c], Y. Slimani [d], T. Chihi [c], B. Ghebouli [e], M. Fatmi [c,*], F. Benlakhdar [f], Saif A. Mouhammad [g], Norah Algethami [g], Sultan Alomairy [g]

[a] Laboratory of Studies Surfaces and Interfaces of Solids Materials, Faculty of Technology, University Ferhat Abbas of Setif 1, Setif, 19000, Algeria
[b] Department of Physics, Faculty of Sciences, University of Mohamed Boudiaf, M'sila, 28000, Algeria
[c] Research Unit on Emerging Materials (RUEM), University Ferhat Abbas of Setif 1, Setif, 19000, Algeria
[d] Laboratory of Intelligent System (LSI), Faculty of Technology, University Ferhat Abbas of Setif 1, Setif, 19000, Algeria
[e] Laboratory for the Study of Surfaces and Interfaces of Solid Materials (LESIMS), University Ferhat Abbas of Setif 1, Setif, 19000, Algeria
[f] Department of Electronic, Faculty of Technology, University of Mohamed Boudiaf, M'sila, 28000, Algeria
[g] Department of Physics, College of Science, Taif University, P.O. Box 11099, Taif, 21944, Saudi Arabia

ARTICLE INFO

Keywords:
Martensitic
Spin-polarized
FePd and FePt
Electronic structure
CASTEP code

ABSTRACT

All studied properties of FeX (X = Pt, Pd) in austenitic and martensitic phases are investigated within Local Spin Density Approximation as exchange functional. The structural parameters at equilibrium for ferromagnetic tetragonal FePt and FePd $a = 3.911$ Å, $c = 3.842$ Å and $a = 3.816$ Å, $c = 3.736$ Å, and the lattice constant for ferromagnetic cubic FePt and FePd $a = 4.9304$ Å and $a = 4.905$ Å agree well with their available theoretical and experimental data. FePd and FePt formation enthalpy of the martensitic phase was −12625.73 eV and −39414.97 eV, while in the austenitic phase it was −12625.33 eV and −39413.97 eV. The rock-salt FePd (tetragonal FePt) is more stable than tetragonal FePd (rock-salt FePt). For both compounds, the anisotropy is more pronounced in the martensitic phase.

1. Introduction

Steel taken at high temperature becomes austenitic, while its cooling at a sufficient rate is martensitic where its hardness is maximal. As soon as the temperature of the super cooled austenitic reaches about 180 °C or lower, a martensitic transformation without diffusion occurs. Martensite is a solid solution of platinum or palladium in saturated Fe-α. The crystal lattice is very distorted and hard. The hardening phenomenon shows a physico-chemical character, where the crystal lattice of Fe-α is highly deformed by the presence palladium or platinum atoms. In hard alloys, the mechanical properties depend on the martensitic phase whose formation mechanism is linked to the quenching medium. Fe–Pt and Fe–Pd alloys are of particular interest because of their interesting mechanical properties and their importance in technology. S.H. Whang et al. establish the phase diagram of Fe–Pt and Fe–Pd systems [1]. To our knowledge; no theoretical study on the martensitic transformation of Fe–Pt and Fe–Pd were carried out. The elaboration and characterization experimentally have been investigated. It is cited as example that Tomáš Káňa et al. modeled Fe–Pt, Fe–Pd and Fe–Cu nanocomposites using Fe nanowires embedded in the fcc Pd, Pt or Cu matrix and the result is that these nanocomposites are stronger than the Pd and Pt matrices [2]. The anomalous Hall effect (AHE) and the Gilbert damping (GD) have been studied theoretically for Fe–Pt and FePd alloys by J. Kudrnovský et al. using the approach of Kubo-Bastin and the non-local couple operator method [3]. Teng X et al. describe a new approach in the fabrication of FePt nanoparticles and granular films ctf having a diameter of 17 nm [4]. In order to create a database for future experimental and theoretical investigations, a theoretical analysis of the structural, elastic, mechanical, electronic, and magnetic properties of FeX (X = Pt, Pd) in the austenitic and martensitic situations was carried out in this work. Anisotropy is present in both phases, but more pronounced in the martensitic one, which is ductile, has an ultra-incompressible characteristic, and can have technological applications. Fe–Pt and Fe–Pd hybridization reduce the total magnetic moment, which is primarily derived from Fe atoms with minor contributions from Pt and Pd sites. FePt and FePd compounds have a metallic behavior for the (spin up) and (spin down) because the Fermi level is occupied and the ferromagnetism comes from the coupling between Fe–Pt and Fe–Pd states. Steel at high

* Corresponding author.
E-mail address: fatmimessaoud@yahoo.fr (M. Fatmi).

https://doi.org/10.1016/j.solidstatesciences.2023.107211
Received 3 April 2023; Received in revised form 30 April 2023; Accepted 11 May 2023
Available online 15 May 2023

Table 1
LSDA equilibrium lattice constant, bulk modulus and its pressure derivative, and cohesive energy of FeX (X = Pd, Pt) in the austenitic and martensitic phases.

Compound	Case	a (Å)	c (Å)	B (GPa)	B′	E_{min} (Ry)
Rock-salt	Ferri	4.9057		157.84	5.86	−12625.64
FePd	Ferro	4.905		157.60	5.82	−12625.64
	Para	4.794		213.70	6.40	−12625.58
Rock-salt	Ferri	4.930		195.98	5.19	−39413.90
FePt	Ferro	4.9304		196.38	5.26	−39413.90
	Ferro	3.94 [9]				
	Para	4.8257		185.33	5.81	−39413.86
Tetragonal	Ferro	3.816	3.736	282	5.72	−12625.73
FePd		3.850 [9]	3.715 [9]			
Tetragonal	Ferro	3.911	3.842	206	5.45	−39414.07
FePt		3.961	3.788			
		[10]	[10]			

temperature becomes austenitic (cfc) and by cooling at a sufficient rate, where the transformation takes place without diffusion, it becomes martensitic (tetragonal) which corresponds to maximum hardness. Martensite is a solid solution of platinum or palladium in saturated iron. It is noted that carbonaceous nitrogen forms with iron a base-centered cubic martensite (bct) during rapid cooling as well as other transition metals such as Zirconium, Titanium and Hafnium which are transformed into a very hexagonal structure hard. The crystal lattice of Fe is highly deformed in the presence of palladium (Pd) or platinum (Pt) atoms. The interesting mechanical properties and their technological importance solicit the choice of Fe–Pt and Fe–Pd alloys, where this characteristic has been verified by ab initio method.

2. Computing technique

The CASTEP simulation program (Cambridge Serial Total Energy Package) was used for all computations [5]. The Schrödinger equations were solved using the functional density theory (DFT) [6] and (LSDA) [7]. During the calculations, we use the norm-conserving pseudo potential to characterize the valence electrons. It handles one situation of the valence layer for Fe ($3d^6 4s^2$), Pd ($4\ d^{10}$) and Pt ($4f^{14}5d^9 6s^1$). The cut-off energy for the plane-wave expansion was set at 380 eV, and the 6 × 6 × 6 set of Monkhorst-Pack mesh was used to sample the Brillouin zone [8]. The Broyden-Fletcher-Goldfarb technique was used to calculate the equilibrium lattice parameter. The fastest technique to identify the lowest energy structure is typically provided by this strategy. In the structural optimization process, the energy change, maximum force, maximum stress and maximum displacement are set as 2.0×10^{-5} eV/atom, 0.05 eV/Å, 0.1 GPa, and 0.002 Å, respectively.

3. Results and discussions

3.1. Structural properties

The crystal structure of FeX (X = Pd, Pt) is described in the rock-salt phase with space group *Fm*"-"3 *m* in the austenitic phase, where Fe occupies (0, 0, 0) position and X atom is located at (1/2, 1/2, 1/2) and in face centered tetragonal (FCT) with space group *P4/mmm* in the martensitic phase, where the unit cell is consist of four atoms: two Fe atoms occupy (0, 0, 0) and (1/2, 1/2, 0) positions, and two X atoms occupy (1/2, 0, 1/2) and (0, 1/2, 1/2) positions. FeX (X = Pd, Pt) lattice constant, bulk modulus and its derivative under pressure, and cohesive energy computed within LSDA approximation in ferromagnetic, ferrimagnetic and paramagnetic states of rock-salt and tetragonal structures are presented in Table 1. The lattice constant of rock-salt FePt in his ferromagnetic phase is larger than that calculated by LDA approach 3.94 Å [9]. Our lattice parameters of face centered tetragonal phase for FePt and FePd are $a = 3.911$ Å, $c = 3.842$ Å and $a = 3.816$ Å, $c = 3.736$ Å. These values agree well with those reported in the literature $a = 3.861$ Å, $c = 3.788$ Å [10] and $a = 3.850$ Å, $c = 3.715$ Å [9]. The difference between austenitic and martensitic is that the primitive lattice of austenitic is a perfect cube, while when transforming into martensitic, this cube deforms so that it is slightly longer than before in one dimension and shorter in the other two. It is schematized in Fig. 1 the effect of volume on total energy for FeX (X = Pt, Pd) in cubic and tetragonal phases at room pressure using LSDA approach. It can be seen that rock-salt FePd is energetically more stable than tetragonal structure FePd and conversely the stability of tetragonal FePt is more pronounced than that of rock-salt FePt.

The chemical potential between atoms has a significant impact on the formation enthalpy of solids. The thermodynamic stability at the ground state is therefore shown by the formation enthalpy's negative value. The lower the formation enthalpy is, the more stability in a system is. The structural stability of FePt and FePd in the cubic and tetragonal phases is studied by examining the enthalpy of formation and the dispersion of phonons [11,12]. As a result, the ground state thermodynamic stability is shown by the formation enthalpy's negative value. The lower the formation enthalpy is, the more stability in a system is [13,14]. The estimation of the thermodynamic stability requires the study of the free energy of the two compounds FePt and FePd in the austenitic and martensitic phases. The evolution of the free energy of the studied compounds under temperature effect in the range 0–1000 K is shown in Fig. 2. The free energy of FePt and FePd in the austenite phase is negative and decreases when the temperature increases. This result implies that these two compounds are thermodynamically stable [12, 15–17]. The stability of *Fm*"-"3 *m* FePt is more pronounced than *Fm*"-"3 *m* FePd. It is noted that the tetragonal structure FePt and FePd becomes

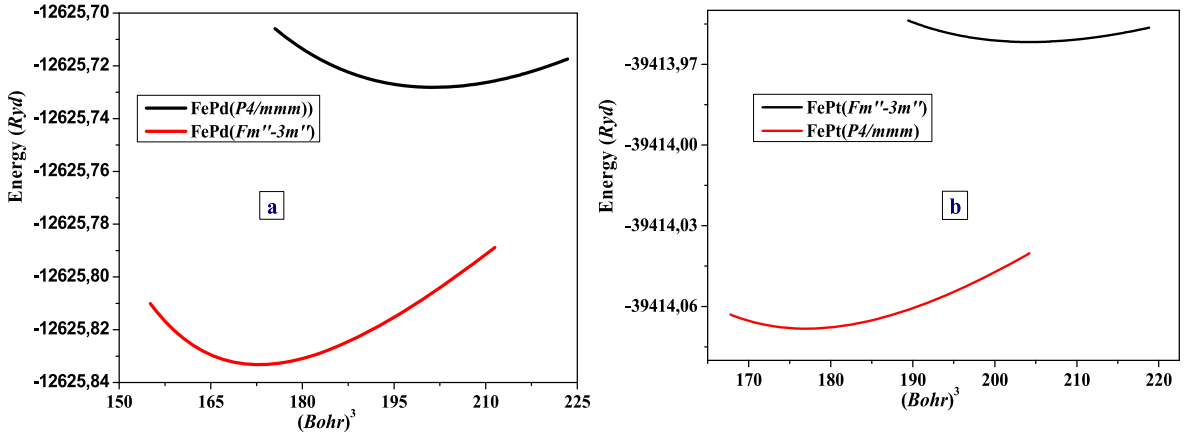

Fig. 1. Effect of volume on total energy for austenitic rock-salt phase (a) and martensitic phase (b) using LSDA.

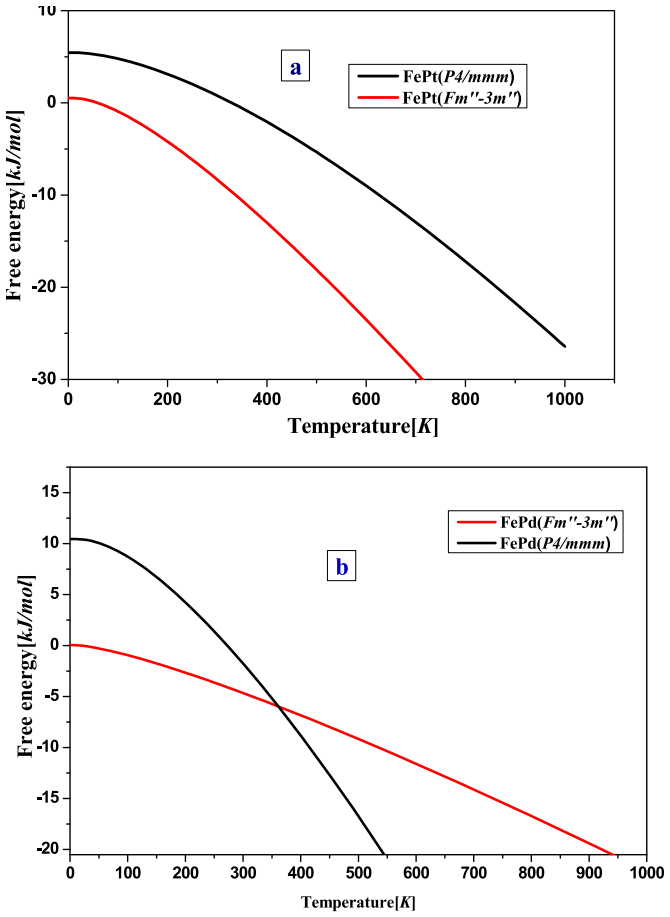

Fig. 2. Effect of temperature on free energy for FePt (a) and FePd (b) using LSDA.

stable at about 300 K. At about 350 K, *P4/mmm* FePd is more stable than *Fm*"-"3 *m* FePd. We study the dynamic stability of FePt and FePd by visualizing the phonon dispersion curves and their total densities of state as shown in Fig. 3 in the austenitic and martensitic phases. The cubic structure shows dynamic instability due to the presence of imaginary phonon frequencies. The *P4/mmm* FePd and *P4/mmm* FePt are dynamic stability. We report in Fig. 4 the electron density difference maps in the plane (100) for FePt and FePd compounds in the austenitic and martensitic phases. In the FePt and FePd cubic structure and FePd tetragonal structure, an Fe atom is surrounded by four first neighbor Pt (Pd) atoms and 4 s neighbor Fe atoms. While the tetragonal FePt structure shows a doublet linear biatomic series of Fe and Pt atoms.

3.2. Elastic and mechanical properties

The stability, stiffness, brittleness, ductility, and anisotropy of a material are described by elastic constants as well as the nature of the forces acting in solids [18]. Elastic constants of FeX (X = Pd, Pt) in the austenitic and martensitic phases calculated within LSDA approximation are reported in Table 2. Seven distinct elastic constants C_{11}, C_{12}, C_{13}, C_{16}, C_{33}, C_{44} and C_{66} make up the tetragonal structure of the martensitic phase. The elastic constants of the tetragonal FePt and FePd are bigger than the cubic FePt and FePd. The bulk modulus of the martensitic phase of FePd is 282 GPa, which is comparable to synthesized ultra-incompressible material PtN_2 having the value 272 GPa [19]. It represents also half of the diamond's experimental value 443 GPa [20]. While the bulk modulus of martensitic phase of FePt is 206 GPa. FePd and FePt are uncompressible, but still less compressible than other iron alloys like iron carbon nitrides and iron silicides [21,22]. The bulk modulus of the rock-salt FePt and FePd obtained from elastic constants is 203 GPa and 163 GPa calculated from the relation $B = \frac{C_{11}+2C_{12}}{3}$, where the relative uncertainty is 3.2% and 3.3%. These results suggest an ultra-incompressible characteristic of the martensitic structure. FePd and FePt are uncompressible, but still less compressible than other iron alloys like iron carbon nitrides and iron silicides [21]. For a tetragonal crystal, the mechanical stability under isotropic pressure leads to restrictions on the elastic constants as follows [23–26]:

$$C_{11}-P>0;\ C_{33}-P>0;\ C_{44}-P>0; C_{66}-P>0;\ \ C_{11}-C_{12}-2P>0;$$
$$(C_{11}+C_{33}-2p)(C_{11}-P)+C_{33}-2C_{13}-3P>0, 2C_{11}+C_{33}+2C_{12}+4C_{13}$$
$$+3P>0$$

The stiffness constants C_{11}, C_{22} and C_{33} are obtained by introducing uniaxial deformations parallel to the crystalline axes. The shear constants C_{44}, C_{55}, C_{66} provide information on the bonds between adjacent planes, hence their usefulness in the stability of the crystal structure. The first distortion C_{11} increases *a* and decreases *b* by the same amount keeping *c* constant. The second distortion increases *a* and decreases *c* keeping *b* constant and finally the last one increases *b* and decreases *c* with *a* constant. The symmetry of the constrained lattice due to these distortions is the same as that of the unconstrained lattice as well as the volume. The martensitic phase exhibits a strong anisotropy because of the martensitic phase's elastic constants C_{11} and C_{33} being much greater than the other elastic constants. Young and Shear Moduli are important mechanical quantities for technological and engineering applications and determine the usefulness of a hard coating material. Hardness and roughness are also determining factors. The hardness of the material is correlated with the shear modulus [27]. Hardness is influenced by the degree of plastic deformation of the material under mechanical load. Young's modulus is defined as the relationship between stress and constraint. Shear modulus is linked to the bending of the bonds, depends on the nature of the bonds and decreases as a function of the ionicity. The shear modulus was derived for the tetragonal-symmetric lattice using the following formula [28–30]:

$$G=\frac{1}{15}(2C_{11}-C_{12}+C_{33}-2C_{13}+6C_{44}+3C_{66})$$

The bulk modulus B_H and the shear modulus G_H were calculated as an arithmetic mean of these extremes; the Voigt and Reuss equations indicate the top and lower limits of the polycrystalline elastic characteristics [31].

$$B=B_H=\frac{B_V+B_R}{2}\quad G=G_H=\frac{G_V+G_R}{2}$$

$$Y=9BG/(3B+G), \nu=(3B-Y)/6B$$

As long as the predicted elastic constants meet the aforementioned requirements, our compounds are mechanically stable. The orientation of the elastic moduli or the sound velocities affects the crystal's elastic anisotropy. Both solid state physics and engineering science can benefit from a good description of this behavior. A number of one indicates that the material is very isotropic, while A value of less than or greater to one indicates that the material is anisotropic. Computation bulk modulus (B), shear modulus (G), Young's modulus (Y), Poisson's ratio ν, B/G ratio and the anisotropy factor (A) of FePd and FePt compounds in the austenite and the martensitic phases, with non-polarized spin are reported in Table 3.

The anisotropy factor of FeX (X = Pd, Pt) martensitic is greater than unity, which reflects the presence of anisotropy. The bulk modulus has the same unit value in both directions, indicating that the crystal is isotropic. Nevertheless, any value other than unity denotes a compressibility along the *c* axis that is smaller or greater than that along the *a* axis. Our results reveal that the bulk modulus along the *c* axis is slightly higher than that of *a* axis. This means that FeX (X = Pd, Pt) martensitic materials are anisotropic. The B/G ratio is a simple

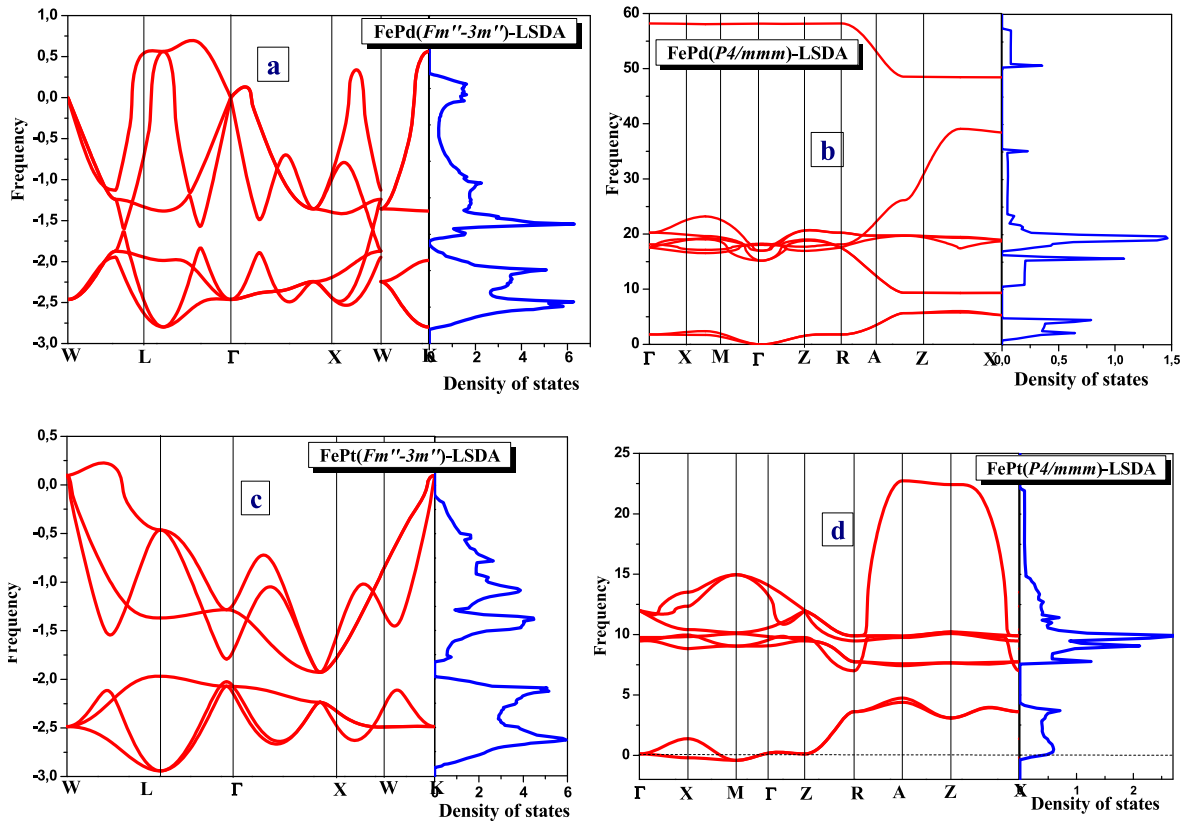

Fig. 3. Phonon dispersion curves and total DOS of FePd and FePt in austenite and martensite phases using phonopy code.

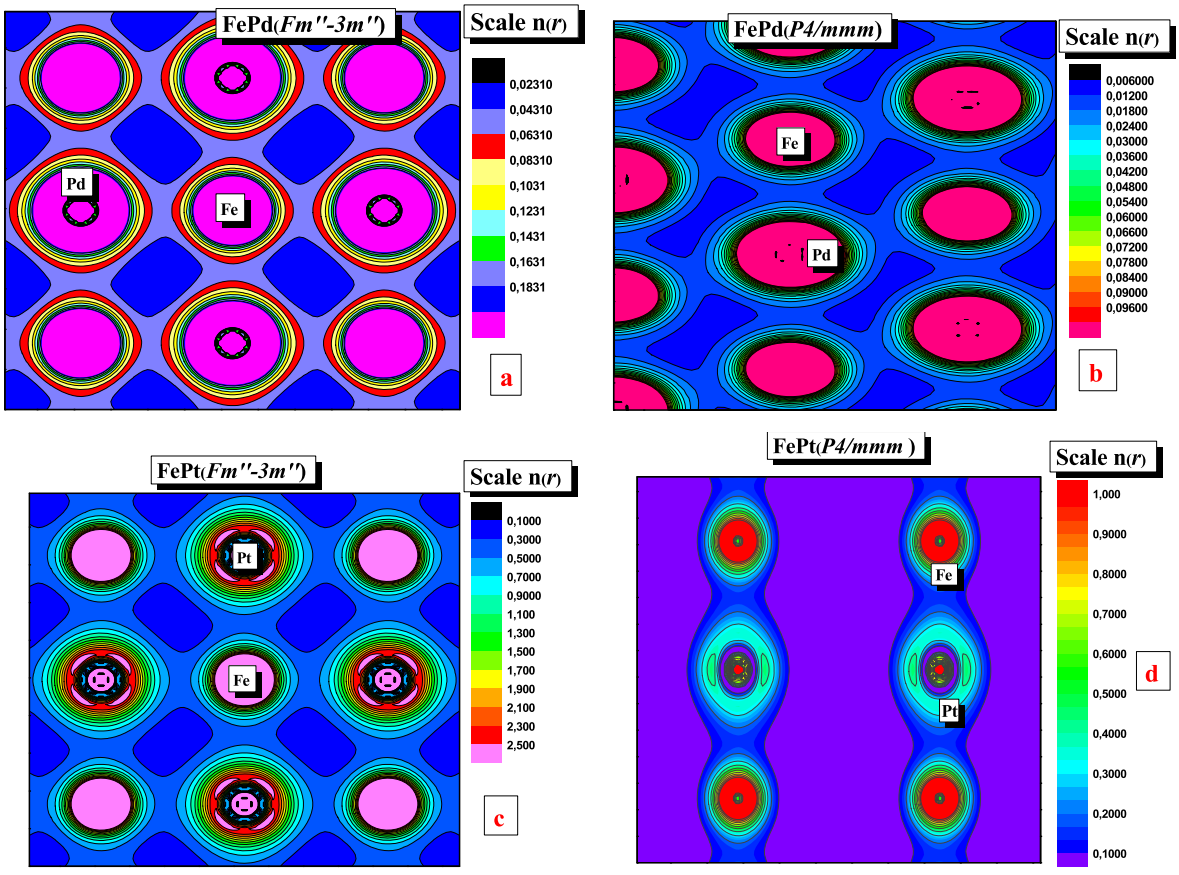

Fig. 4. Electron density for FePt (*Fm*"-"3 *m*) and FePt (*P4/mmm*) using LSDA.

Table 2
Elastic constants of FeX (X = Pd, Pt) in the austenite and the martensitic phases.

Compound	C_{11} (GPa)	C_{33} (GPa)	C_{44} (GPa)	C_{66} (GPa)	C_{12} (GPa)	C_{13} (GPa)
Rock-salt FePd	363		−13		63	
Tetragonal FePd	312	315	158	138	153	155
Rock-salt FePt	419		3		95	
tetragonal FePt	442	403	180	203	203	190

relationship related to brittle or ductile behavior of materials; it has been proposed by Pugh [32]. A high B/G ratio is associated with ductility, whereas a low value corresponds to the brittleness. The critical value separating ductile and brittle material is 1.75. For example, diamonds have a B/G of 0.80 [33], while Al, Co, Rh and Ir have B/G ratios of 2.74, 2.43, 1, 77 and 1.74, respectively [32]. Our calculated B/G ratios for martensitic compounds, we get 1.77 and 1.79 for the martensitic compounds FePd and FePt. The fact that martensitic state is ductile and can have technological applications. Together with B/G, it is generally known that (C_{11}–C_{12}) and *Y* play important roles in determining a material's mechanical properties [34]. By emphasizing that for the martensitic compounds FePd and FePt, the calculated values are 159 GPa and 239 GPa and Young's modulus 295 GPa and 85 GPa, martensite most probably has a much poorer plasticity. It should be noted that $C_{66} < C_{44}$, this suggests that shearing [100] (001) is simpler than [100] (010) to shear the martensitic phase. Increasing pressure reduces hardness, unlike B, Y, G and B/G ratio, which increase monotonously [35].

3.3. Electronic and magnetic properties

The electronic and magnetic properties of FeX (X = Pd, Pt) in the

Table 3
Elastic parameters of FePd and FePt in the austenite and martensitic phases (with non-polarized spin).

Species	B (GPa)	B_R (GPa)	B (GPa)	G_V (GPa)	G_R (GPa)	G (GPa)	Y (GPa)	ν	B/G	A	k_c/k_a
Rock-salt FePd	163	163	163	52	−23	14	343		0.47		
Tetragonal FePd	207	207	207	123	111	117	295	0.26	1.76	1.98	0.96
Rock-salt FePt	203	203	203	66	5	36	283		5.64		
Tetragonal FePt	272	272	272	155	148	152	85	0.44	1.78	1.50	1.24

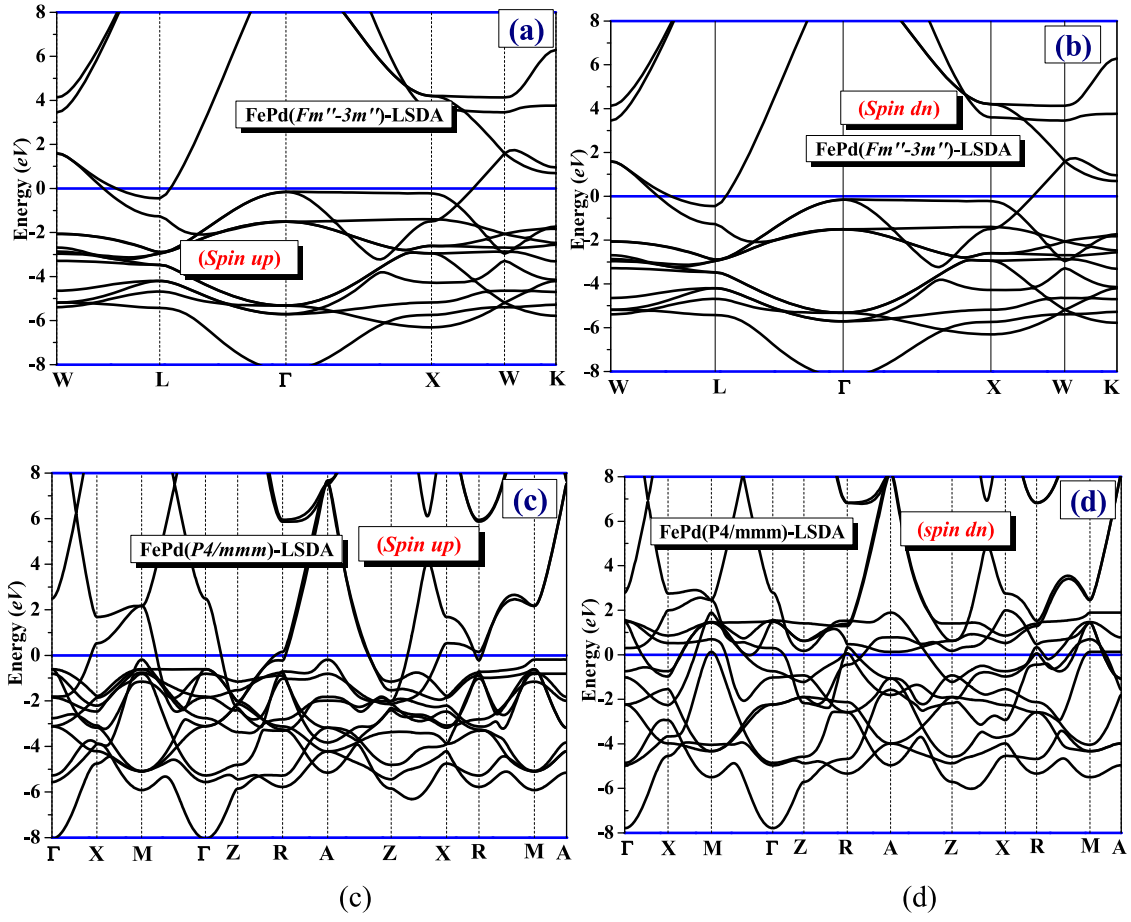

Fig. 5. Band structures of rock-salt FePd in spin up (a), spin dn (b) and tetragonal FePd in spin up (c), spin dn (d) using LSDA.

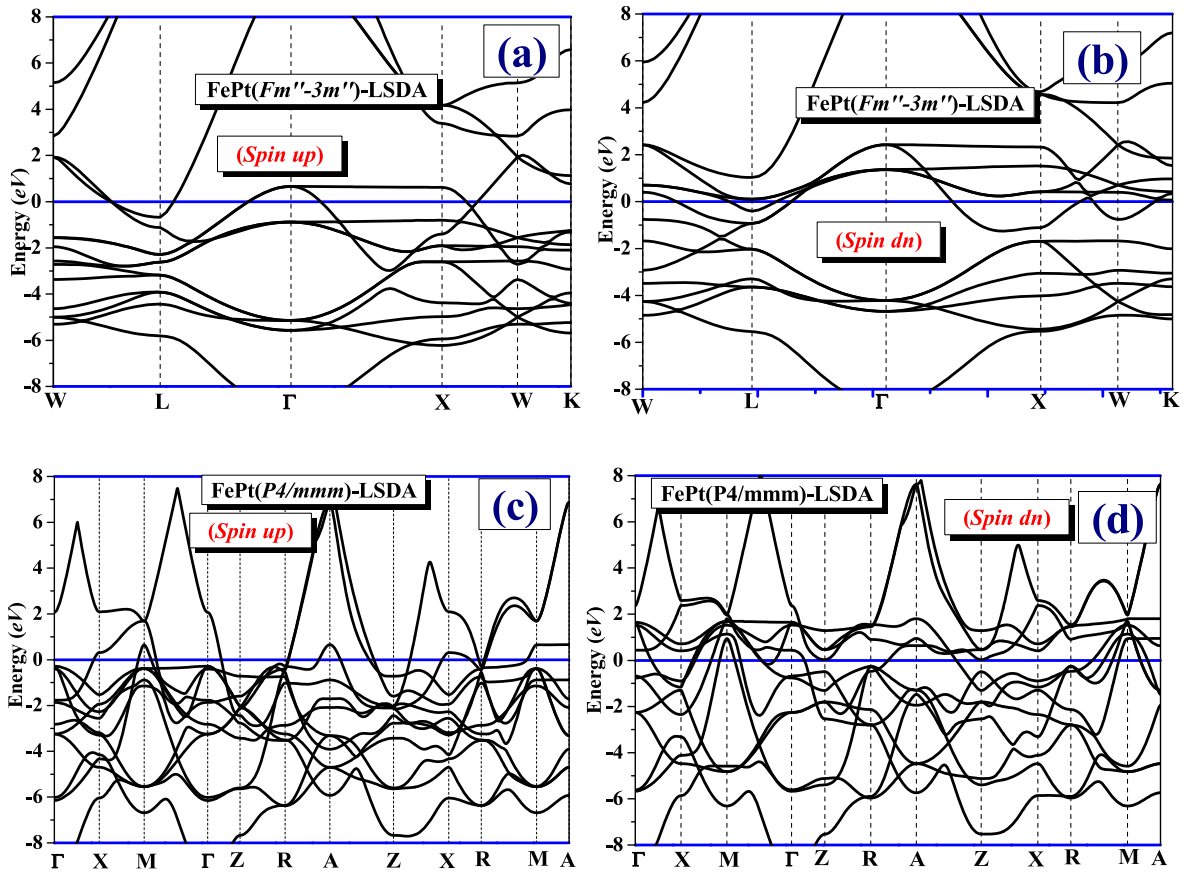

Fig. 6. Band structures of rock-salt FePt in spin up (a), spin dn (b) and tetragonal FePt in spin up (c), spin dn (d) using LSDA functional.

austenite and martensitic phases are discussed in this subsection. The spin-polarized density of states (DOS) and band structure calculations are performed using LSDA scheme at their equilibrium ferromagnetic lattice parameters. It should be stated that DFT under LDA tends to underestimate the bandgap energy [36]. The spin direction (↓ and ↑) is used to represent the spin directions of Fe (down and up). The spin-polarized band structures of FePt and FePd in the austenite and martensitic phases for the spin up and spin down within LSDA and GGA + U are plotted in Fig. 5 to 8. All spectra show a metallic character. The band structure of FePt with spin-orbit coupling shows several bands crossing the Fermi level. The valence bands are formed as continuous board along the Γ-X lines in the austenite phase of FePt and FePd in the spin up and spin dn cases. The continuous board formed is positioned above the Fermi level for FePt at energy 0.8 eV and 2.5 eV, and just at the Fermi level at the top of the valence band in the FePd case. The continuous board in the martensitic phase are distributed everywhere in the BZ for both spin up and spin dn. The knowledge of the contribution of the different sites in the valence and conduction bands and the manifest ferromagnetism in these compounds requires the computation of the partial electronic density of state. It was observed that increasing the value of U in the GGA + U increased the stabilization energy for ferromagnetic ordering. Tetragonal and cubic FePt and FePd have 100% spin polarization, and zero band gap crossing points in both spin directions, hence their potential applications in spintronics [37]. The spin-polarized full and partial state densities of FePt and FePd in the austenite and martensitic phases for the spin up and spin down are plotted in Fig. 9. Due to the Fermi level being occupied, it can be seen that all spin-polarized band structures exhibit metallic behavior for both the (spin up) and (spin down). The PDOS and TDOS spectra in FePt and FePd compounds in the austenite and martensitic phases for the spin up and spin down are symmetrical with respect to the horizontal axis, with exception of FePd in the austenite phase. The contribution to the magnetic moment in all compounds is mainly due to Fe-3d electrons for the spin up. The Pt-5d/6s and Pd-4d states contribute little to the magnetic moment for FePt and FePd compounds in the austenite and martensitic phases. The conduction band for the spin up is empty for FePt and FePd in austenite and martensitic phases. Table 4 lists the total and local magnetic moments that were calculated using LSDA for a variety of Fe, Pt, and Pd sites for FePt and FePd in the austenite and martensitic phases. The ferromagnetism in FePt and FePd compounds comes from the coupling between Fe–Pt and Fe–Pd states. Parallel to the Pt and Pd moments is the magnetic moment of Fe. Fe–Pt and Fe–Pd hybridization reduce the total magnetic moment, which is primarily obtained from Fe atoms with modest contributions from Pt and Pd sites. The GGA + U overestimated the value of magnetic moment and could attain the experimental value of magnetic moment for negative U values [38]. Hubbard's parameter Ueff = 3 eV is chosen for the all studied transition metals, then Hubbard's coefficient was chosen U = 3 eV for Fe and Pt. In the case of an Pd (d^{10}) atom, the orbit is full and therefore Hubbard's coefficient was chosen U = 0. Tetragonal and cubic FePt and FePd have 100% spin polarization, and zero band gap crossing points in both spin directions, hence their potential applications in spintronics. The strong Coulomb repulsion between electrons was corrected using the Hubbard parameter *U*, which ranged from 2 to 6 eV for Fe 3*d*. The calculated band structure and density of states indicated that the on-site Coulomb repulsion *U* significantly influenced the hybridization of Pt 2*p* (Pd 2 d) with Fe 3*d* orbitals at the valence and conduction bands. We investigated the austenite FePd compound's partial electronic density of state for spin up and spin down, as depicted in Fig. 10. The density of state of the iron atom in the spin up is high in the valence band compared to the case of the spin down, whereas in the conduction band the reverse is observed. The palladium atom presents in up and down spins a high density.

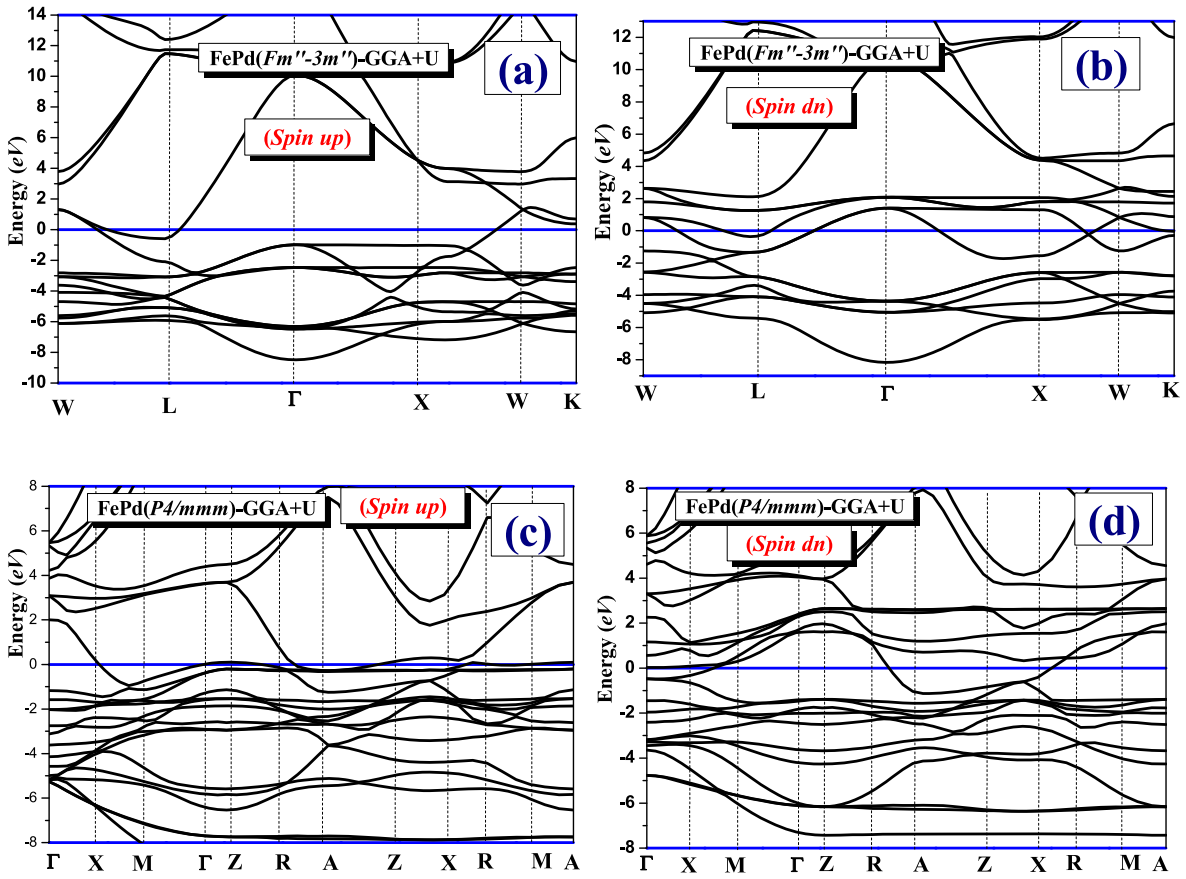

Fig. 7. Band structures of rock-salt FePd in spin up (a), spin dn (b) and tetragonal FePt in spin up (c), spin dn (d) using GGA + U functional.

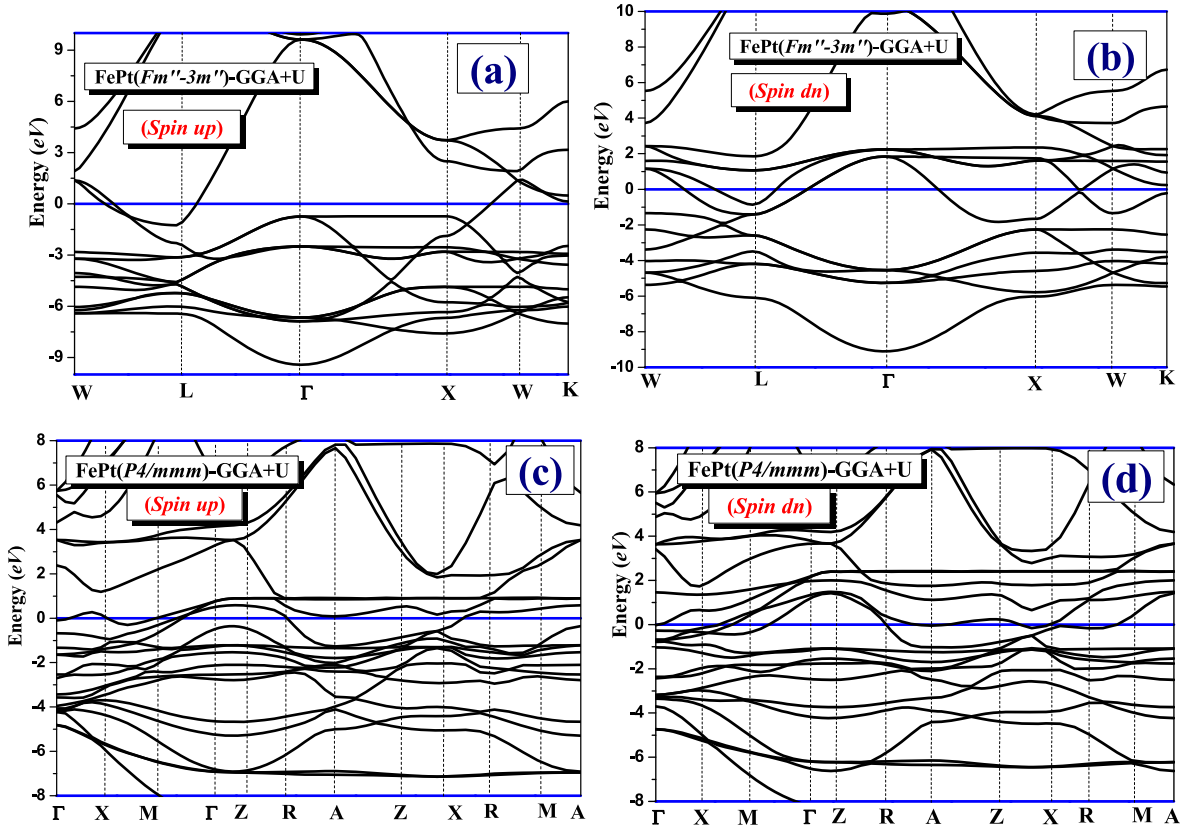

Fig. 8. Band structures of rock-salt FePt in spin up (a), spin dn (b) and tetragonal FePt in spin up (c), spin dn (d) using GGA + U functional.

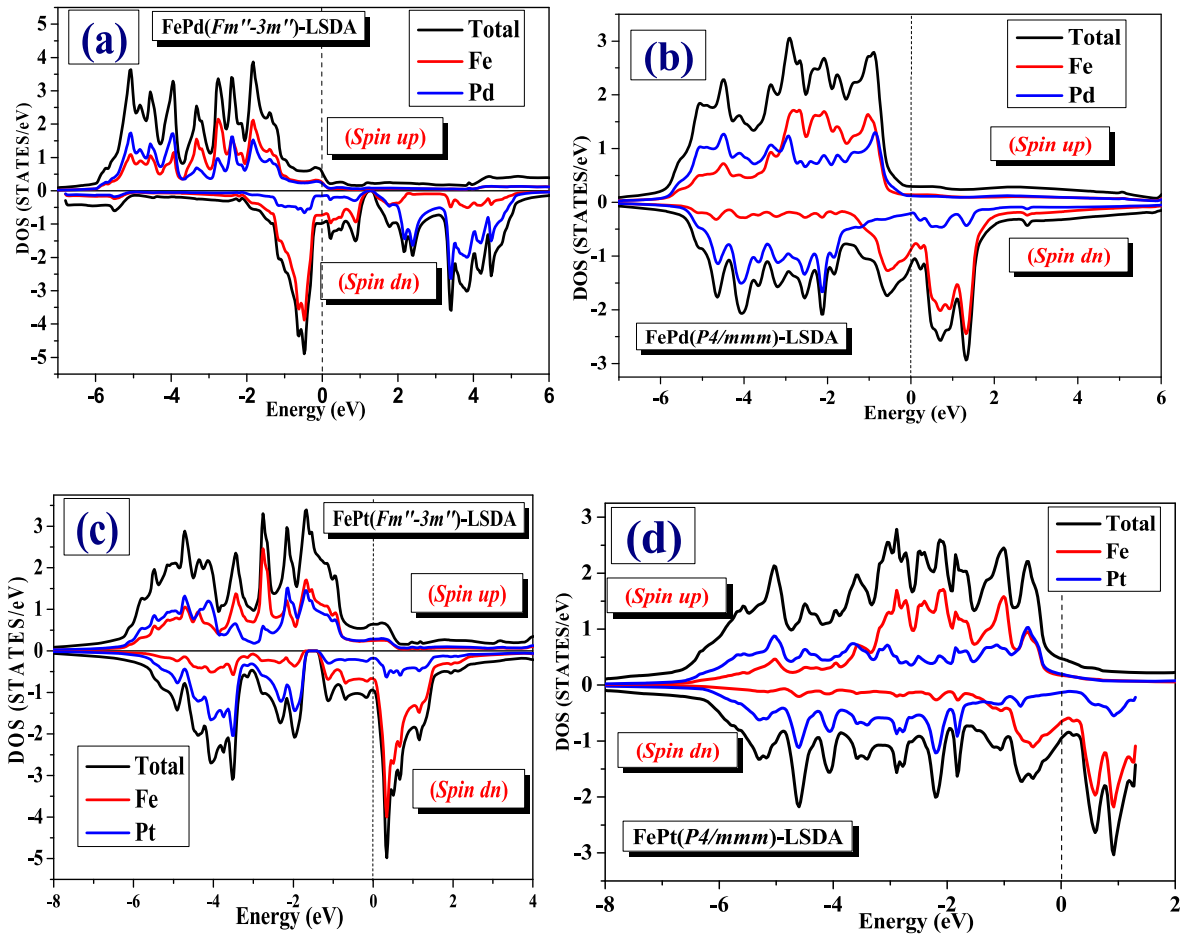

Fig. 9. The spin-polarized total and partial state densities of FePt and FePd in the austenite a nd martensitic phases for the spin up and spin down.

Table 4
Contribution of Fe, Pd and Pt to the magnetic moment of FePt and FePd in the austenite and martensitic phases using LSDA.

Compounds	$\mu_{interstitial}$ (μ_B)	μ (Fe) (μ_B)	μ (X) (μ_B)	μ_{Tot} (μ_B)
Rock-salt FePd	0.04165	3.15119	0.43040	3.62323
Tetragonal FePd	−0.05147	2.92370	0.34356	3.21579
Rock-salt FePt	0.05293	2.93551	0.39424	3.38268
Tetragonal FePt	0.03213	2.79031	0.35545	3.17789

4. Conclusion

We present an ab-initio study on the structural, mechanical, electronic and magnetic properties of FeX (X = Pd, Pt). The crystal structure is described with space group *Fm*"-"3 *m* and *P4/mmm* in the austenitic and martensitic phases. The symmetry of the constrained lattice due to the distortions is the same as that of the unconstrained lattice. The band structure of FePt with spin-orbit coupling shows several bands crossing the Fermi level. Because to the Fermi level being occupied, all spin-polarized band structures exhibit metallic behavior for both the majority spin (spin up) and minority spin (spin down). The ferromagnetism in FePt and FePd compounds comes from the coupling between Fe–Pt and Fe–Pd states. The valence bands are formed as continuous board along the Γ-X lines in the austenite phase of FePt and FePd in the spin up and spin dn cases. Fe–Pt and Fe–Pd hybridization reduce the total magnetic moment, which is primarily obtained from Fe atoms with modest contributions from Pt and Pd sites. The contribution to the magnetic moment in all compounds is mainly due to Fe-3d electrons for the spin up, while Pt-5d/6s and Pd-4d states contribute little for FePt and FePd in the austenite and martensitic phases.

Authors statements

Conceptualization: Bouferrache, Data curation: M. Ghebouli, Formal analysis:B. Ghebouli and Y. Slimani, Methodology:T. Chihi, Software:M. Ghebouli, Validation: Saif A. Mouhammad, Visualization: Norah Algethami, Sultan Alomairy[5], Roles/Writing - original draft: M. Fatmi, Z. Zerrougui, Writing - review & editing: M. Fatmi

Declaration of competing interest

The authors whose names are listed immediately below certify that they have NO affiliations with or involvement in any organization or entity with any financial interest (such as honoraria; educational grants; participation in speakers' bureaus; ember ship, employment, consultancies, stock ownership, or other equity interest; and expert testimony or patent-licensing arrangements), or non-financial interest (such as personal or professional relationships, affiliations, knowledge or beliefs) in the subject matter or materials discussed in this manuscript.

Data availability

No data was used for the research described in the article.

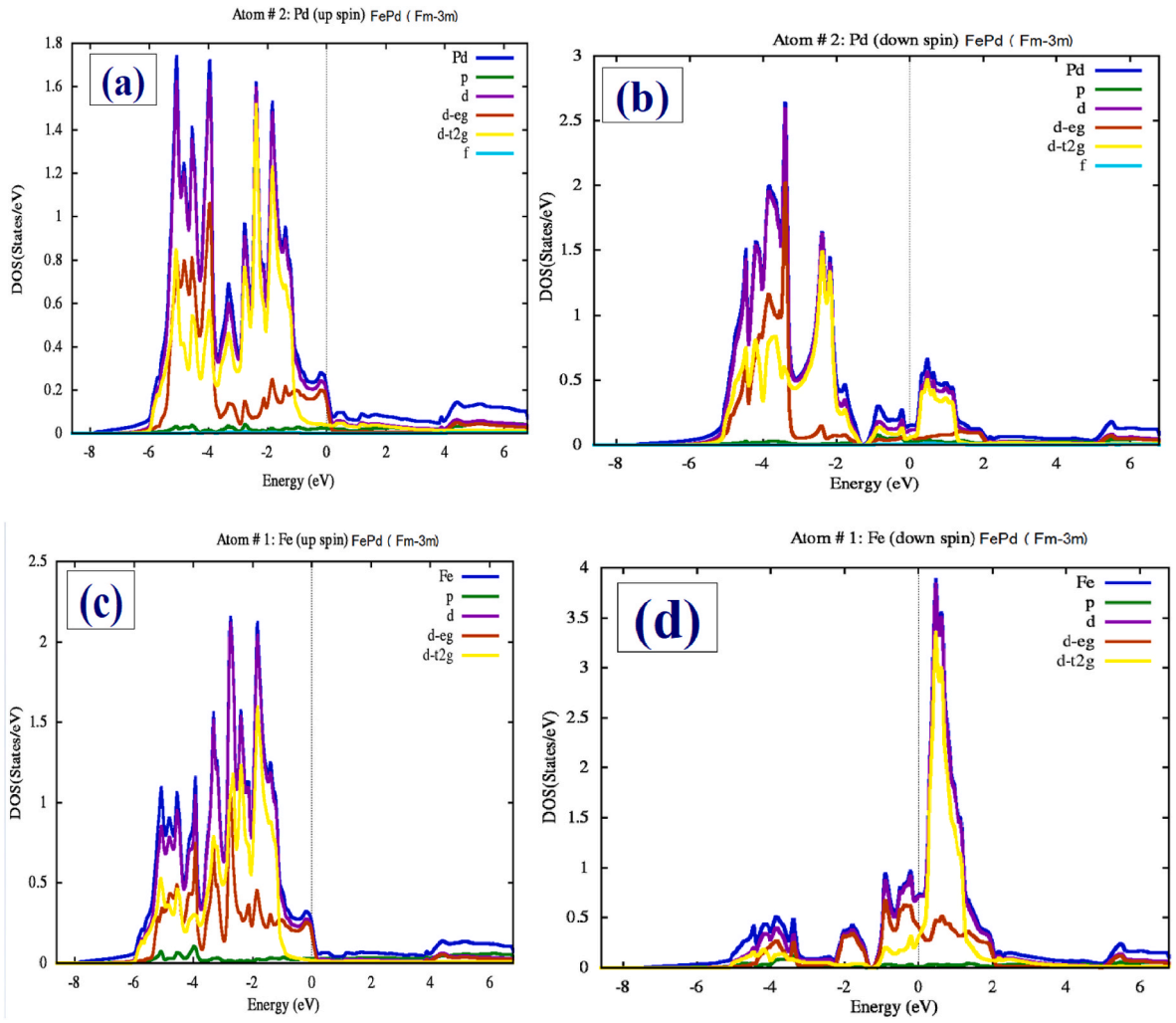

Fig. 10. Partial density of states rock-salt FePd using LSDA.

Acknowledgements

The researchers would like to acknowledge deanship of scientific research, Taif University for funding this work.

References

[1] S.H. Whang, Q. Feng, Y.Q. Gao, Acta Mater. 46 (18) (1998) 6485–6495.
[2] K. Tomáš, Z.M. Černý, M. Mojmír, Journal of Magnetism and Magnetic Materials vol. 469, 2019, pp. 100–107.
[3] J. Kudrnovský, V. Drchal, I. Turek, Spin-orbit driven phenomena in the isoelectronic L10-Fe(Pd,Pt) alloys from first principles, Phys. Rev. B 96 (2017), 214437.
[4] X. Teng, H. Yang, Synthesis of face-centered tetragonal FePt nanoparticles and granular films from Pt@Fe2O3 Core−Shell nanoparticles, J. Am. Chem. Soc. 47 (2003), 14559, 125.
[5] M.A. Ghebouli, B. Ghebouli, T. Chihi, M. Fatmi, Russ. J. Phys. Chem. A 95 (2) (2021) 296–306.
[6] P. Hohenberg, W. Kohn, Phys. Rev. B 13 (1964) 6 864.
[7] S.A. Dar, M.A. Ali, V. Srivastava, Eur. Phys. J. B 93 (2020) 1–11.
[8] H.J. Monkhorst, J.D. Pack, Phys. Rev. B 13 (1976) 5188.
[9] M.S. Seehra, V. Singh, P. Dutta, S. Neeleshwar, Y.Y. Chen, C.L. Chen, S.W. Chou, C. C. Chen, J. Phys. D Appl. Phys. 43 (2010), 145002.
[10] T. Chihi, M. Fatmi, B. Ghebouli, M.A. Ghebouli, Chin. J. Phys. 54 (1) (2017) 127–134.
[11] Y. Xu, Z. Cai, P. Du, J. Zhou, Y. Pan, P. Wu, C. Cai, J. Mater. Chem. A. 10 (2022), 24866.
[12] Y. Pan, J. Phys. Chem. Solid. 174 (2023), 111152.
[13] Y. Pan, M. Wen, L. Wang, X. Wang, Y.H. Lin, W.M. Guan, J. Alloys Compd. 648 (5) (2015) 771–777.
[14] Y. Pan, J.M. Guo, Y.H. Lin, W.Y. Liu, ShL. Wang, K.H. Deng, J. Alloys Compd. 621 (5) (2015) 201–205.
[15] Y. Pan, E. Yu, Int. J. Hydrogen Energy 7 (64) (2022), 27608.
[16] E. Yu, Y. Pan, J. Chem. 46 (2022), 24866.
[17] S. Chen, Y. Pan, Appl. Surf. Sci. 599 (2022), 154041.
[18] S. Boucetta, J. Magnesium Alloys 2 (2014) 59.
[19] R. Yu, Q. Zhan, X.F. Zhang, Appl. Phys. Lett. 88 (2006), 051913.
[20] G. Calzaferri, R. Rytz, J. Phys. Chem. 100 (1996), 11122.
[21] D. Errandonea, J. Ruiz-Fuertes, J.A. Sans, D. Santamaría-Perez, O. Gomis, A. Gómez, F. Sapiña, Phys. Rev. B 85 (2012), 144103.
[22] D. Errandonea, D. Santamaría-Perez, A. Vegas, J. Nuss, M. Jansen, P. Rodríguez-Hernandez, A. Muñoz, Phys. Rev. B 77 (2008), 094113.
[23] Zhengquan Hu, Weiwei Xu, Cai Chen, Yufeng Wen, Lili Liu, Adv. Mater. Sci. Eng. 5 (2018) 1–9.
[24] F. Mouhat, F.X. Coudert, Phys. Rev. B 90 (22) (2014), 224104.
[25] H.C. Zhai, X.F. Li, J.Y. Du, Mater. Trans. 53 (7) (2012) 1247–1251.
[26] D.C. Wallace, Thermodynamics of Crystals, Wiley, New York, USA, 1972.
[27] D.M. Teter, Mater, Res, Soc, Bull 23 (1998) 22.
[28] S.A. Saoucha, I. Bouchama, S. Alomairy, M.A. Ghebouli, B. Ghebouli, M. Fatmi, Solid State Commun. 354 (2022), 114897.
[29] M.A. Ghebouli, B. Ghebouli, L. Krache, S. Alomairy, M. Fatmi, T. Chihi, M. Reffas, Bull. Mater. Sci. 45 (3) (2022) 124.
[30] Y. Naceur, H. Bourbaba, M.A. Ghebouli, L. Krache, B. Ghebouli, T. Chihi, M. Fatmi, Sultan Alomairy, Scientific Reports 12 (1) (2022) 1–13.
[31] K. Bouferrache, M.A. Ghebouli, B. Ghebouli, M. Fatmi, Sultan Alomairy, T. Chihi, Chin. J. Phys. 81 (2023) 303–324.
[32] K. Bouferrache, L. Krache, M.A. Ghebouli, B. Ghebouli, Sameh I. Ahmed, M. Fatmi, T. Chihi, B. Gueridi, Chem. Phys. Impact 5 (2022), 100110.

[33] J. Haines, J.M. leger, G. Bocquillon, Synthesis and design of superhard materials, Annu. Rev. Mater. Res. 31 (2001) 1–23.
[34] A. Sumer, J.F. Smith, J. Appl. Phys. 33 (1962) 2283.
[35] Y. Pan, Y.H. Lin, M. Wen, Q.N. Meng, RSC Adv. (109) (2014), 63891.
[36] T. Ouahrani, R.M. Boufatah, M. Benaissa, Á. Morales-García, M. Badawi, D. Errandonea, Phys. Rev. Mater. 7 (2023), 025403.
[37] J. Wang, H. Yuan, Y. Liu, X. Wang, G. Zhang, Phys. Rev. B 106 (2022) L060407.
[38] G. Ding, J. Wang, Z.M. Yu, Z. Zhang, W. Wang, X. Wang, Phys. Rev. Mater. 7 (2023), 014202.